

Abstract

Carboxylic acids are ubiquitous in atmospheric particles, and they play an important role in the physical and chemical properties of aerosol particles. During measurements in coastal California in the summer of 2009, carboxylic acid functional groups were highly associated with trajectories from an industrial region with high organic mass (OM), likely from fossil fuel combustion emissions. The concentration of carboxylic acid groups peaked during daytime, suggesting a photochemical secondary formation mechanism. This daytime increase in concentration was tightly correlated with O_3 mixing ratio, indicating O_3 was the likely driver in acid formation. Based on the diurnal cycles of carboxylic acid and alkane groups, the covariation of carboxylic acid groups with O_3 , and the composition of the Combustion factor resulted from the factor analyses, gas-phase alkane oxidation by OH radicals to form dihydrofuran followed by further oxidation of dihydrofuran by O_3 is the likely acid formation mechanism. Using the multi-day average of the daytime increase of carboxylic acid group concentrations and m/z 44-based Aged Combustion factor, we estimated the lower-bound contributions of secondary organic aerosol (SOA) formed in 12-h daytime of processing in a single day to be 30% of the carboxylic acid groups and 25–45% of the Combustion factor concentration. These unique ambient observations of photochemically-driven acid formation suggest that gas-phase alkanes might be important sources of SOA formation in this coastal region.

1 Introduction

Organic compounds typically account for 10–70% of dry particle mass (Turpin et al., 2000). Understanding the chemistry of particle-phase organic compounds is important for assessing the effects of aerosol particles on air quality, human health, and climate change (Fuzzi et al., 2006). The major organic components identified in ambient particles include alkane, carboxylic acid, hydroxyl, amine, and non-acid carbonyl functional

Ozone-driven formation of acid

S. Liu et al.

Title Page

Abstract

Introduction

Conclusions

References

Tables

Figures

◀

▶

◀

▶

Back

Close

Full Screen / Esc

Printer-friendly Version

Interactive Discussion



groups (Maria et al., 2002; Liu et al., 2009; Russell et al., 2009a). Alkane groups, a large component of ambient organic compounds (Maria et al., 2002), are typically associated with primary gas and particle-phase emissions that originate from fossil fuel combustion emissions, including vehicular exhaust (Rogge et al., 1993) and coal burning (Wang et al., 2009). In addition to being prevalent in primary emissions, alkane groups remain in many oxygenated secondary organic products, e.g. β -pinene oxidation products might include norpinic acid (Yu et al., 1999), which has two oxygenated groups and five hydrogenated carbons, each with 1–3 C-H bonds. Carboxylic acid groups are observed in urban, rural, and remote atmospheric particles and sometimes account for more than 30% of OM (Grosjean et al., 1978; Kawamura and Gagosian, 1987; Kawamura, 1993; Fraser et al., 2002; Wang et al., 2002; Sullivan and Weber, 2006; Claeys et al., 2007; Russell et al., 2009a; Wang et al., 2009; Zhang et al., 2010). Because many carboxylic acids are highly soluble and tend to absorb water under high relative humidity (RH), they could affect physical (e.g. light scattering) and chemical (e.g. aqueous-phase reaction) properties of ambient particles. Carboxylic acid groups are generally SOA components. For example, enhanced abundance of ambient carboxylic acids in summer and in the afternoon suggests that carboxylic acids are formed by photochemical oxidation in the atmosphere (Kawamura and Ikushima, 1993; Kawamura and Yasui, 2005). Laboratory studies have shown condensed-phase carboxylic acid groups formed as secondary organic aerosols (SOA) from anthropogenic and biogenic precursors (Yu et al., 1999; Fisseha et al., 2004; Claeys et al., 2007). Aqueous-phase or in-cloud formation of carboxylic acids has been suggested by several field studies and modeling simulations (Blando and Turpin, 2000; Warneck, 2003; Ervens et al., 2004; Yu et al., 2005; Sullivan and Prather, 2007; Altieri et al., 2006), indicating carboxylic acid groups can be formed through various processes under different ambient conditions. Recently, alkane reactions have been studied by several research groups (Hallquist et al., 2009; Lim and Ziemann, 2009; Miracolo et al., 2010; Presto et al., 2010). Russell et al. (2011) proposed formation of carboxylic acid groups from alkane groups via photochemical oxidation.

**Ozone-driven
formation of acid**

S. Liu et al.

Title Page

Abstract

Introduction

Conclusions

References

Tables

Figures

◀

▶

◀

▶

Back

Close

Full Screen / Esc

Printer-friendly Version

Interactive Discussion



**Ozone-driven
formation of acid**

S. Liu et al.

Title Page

Abstract

Introduction

Conclusions

References

Tables

Figures

I◀

▶I

◀

▶

Back

Close

Full Screen / Esc

Printer-friendly Version

Interactive Discussion



Large uncertainty in SOA formation mechanisms makes identification of ambient SOA controversial. Organic carbon (OC) to elemental carbon (EC) ratio has been used to estimate SOA by assuming an average OC/EC from emission source measurements. OC/EC exceeding the average OC/EC is assumed to be SOA (Turpin et al., 1991). The SOA mass estimated from this method is highly uncertain, since OC/EC is highly variable from source to source (Gray et al., 1986) and the average OC/EC is dependent on meteorological conditions. Another approach is to identify SOA products from individual precursors (Yu et al., 1999). This method requires detection of SOA by molecular level speciation and known SOA formation mechanisms, which are often not available.

In this work, organic functional groups are quantified using Fourier Transform Infrared spectroscopy (FTIR) and organic mass fragments are measured using Aerosol Mass Spectrometry (AMS) at a coastal site in southern California. Because of the frequent and consistent aerosol transport from the shipping activities at Los Angeles and Long Beach, the measurements provide an opportunity to use the diurnal trend in aerosol composition to evaluate the contribution of SOA. The formation mechanism of carboxylic acid groups and other oxygenated organic aerosol (OOA) is also considered based on the recurrence of diurnal cycles.

2 Sample collection and instrumentation

Submicron particles were continuously collected at the Scripps Pier (8 m above sea level) in La Jolla (32.87° N, 117.25° W), California, from 15 August to 1 October 2009. Instruments were deployed in a temperature-controlled container at the end of the pier (300 m west of the shoreline) and shared a common 3/8" o.d. stainless steel inlet. Submicron particles were separated by a PM₁ cyclone and were collected on four filters daily for the time periods: 06:00–10:00, 10:00–14:00, 14:00–18:00, and 18:00–06:00 (the next day) Pacific Standard Time (PST, one hour earlier than local daylight time), representing morning, midday, afternoon, and nighttime samples, respectively. A 24-h

**Ozone-driven
formation of acid**

S. Liu et al.

[Title Page](#)[Abstract](#)[Introduction](#)[Conclusions](#)[References](#)[Tables](#)[Figures](#)[◀](#)[▶](#)[◀](#)[▶](#)[Back](#)[Close](#)[Full Screen / Esc](#)[Printer-friendly Version](#)[Interactive Discussion](#)

sample was simultaneously collected in parallel with shorter samples for each day. 37 mm Teflon filters (Teflo, Pall Inc., Ann Arbor, MI) were used for the FTIR analysis performed using a Bruker Tensor 27 FTIR Spectrometer with a DTGS detector (Bruker, Waltham, MA). Samples were frozen during storage to reduce desorption. Each Teflon filter was scanned before and after sampling using the FTIR and the pre-scanned spectrum was subtracted from the post-scanned spectrum to correct for variability in the polytetrafluoroethylene (Teflon) absorption of the Teflon filters. An automated algorithm was used to conduct spectrum subtraction, baselining, peak-fitting, and error estimation (Russell et al., 2009a). Mass concentrations of alkane, carboxylic acid, hydroxyl, amine, non-acid carbonyl, organonitrate, alkene, and aromatic functional groups were quantified using previously reported algorithms and standards (Russell et al., 2009a; Day et al., 2010).

Concentrations of non-refractory organics, sulfate, ammonium, nitrate, and chloride in submicron particles were measured using a quadrupole AMS (Aerodyne, Billerica, MA). In this instrument, particles passed through a 100 μm orifice are focused by an aerodynamic lens followed by vaporization (600 $^{\circ}\text{C}$) and ionization at the entrance of a quadrupole mass spectrometer. Particle size is measured by time-of-flight between a rotating chopper, which modulates the particle beam (Jayne et al., 2000). The “mass spectrum” (MS) mode and the “time-of-flight” (TOF) mode alternated during the measurements. Complete mass spectra (1–300 amu) and size distributions for selected mass fragments were stored at 5-min resolution. Transmission efficiency was approximately 100% for 60 to 600 nm particles (Jayne et al., 2000). Dry ammonium nitrate particles (350 nm) were used to calibrate the ionization efficiency weekly. Collection efficiency (CE) of the AMS was assigned to each 5-min organic and inorganic measurements to correct for particle loss due to bouncing off the vaporizer. The CE (ranging from 0.45 to 1) was determined as a linear function of ammonium to sulfate molar ratio, with 0.45 and 1 corresponding to ratios 1 and 0, respectively (Quinn et al., 2006). The campaign average ammonium to sulfate molar ratio was 1.9 ± 1.2 , and the CE was 0.45 for approximately 85% of the measurements.

**Ozone-driven
formation of acid**

S. Liu et al.

[Title Page](#)[Abstract](#)[Introduction](#)[Conclusions](#)[References](#)[Tables](#)[Figures](#)[◀](#)[▶](#)[◀](#)[▶](#)[Back](#)[Close](#)[Full Screen / Esc](#)[Printer-friendly Version](#)[Interactive Discussion](#)

Single particles were impacted on Si_3N_4 windows on 27 August and 4, 14, 20, and 22 September. Four samples were collected (15–30 min) on these days for periods overlapping the four FTIR filter sampling periods. Samples were stored at temperatures below 0°C before analysis at the Advanced Light Source (Lawrence Berkeley National Laboratory, CA) on beamline 5.3.2 (Liu et al., 2009). Single particle image and K-edge X-ray absorption spectrum were acquired using a combination of Scanning Transmission X-ray Microscopy (STXM) and Near-Edge X-ray Absorption Fine Structure (NEXAFS) spectroscopy. Organic functional groups (including alkane, hydroxyl, ketone, alkene, and carboxylic acid groups) and inorganic potassium and carbonate of carbon-containing single particles were measured (Russell et al., 2002; Maria et al., 2004). Particle size, image, and organic functional group abundance were analyzed using an automated algorithm described by Takahama et al. (2010).

Carbon monoxide (CO) dry air mole fractions were measured by a newly installed Horiba APMA-370 NDIR analyzer. Air was continuously pumped through a sampling line (400 m; $1/2''$ Dekabon) with an inlet 20 m a.s.l. Measurements were reported as 5-min averages, initially using the factory calibration. The instrument was subsequently calibrated against standards on the NOAA/ESRL 2004 CO calibration scale, and the field campaign results were recalculated based on the measurement of a whole air reference cylinder that was measured during the field campaign and also during the NOAA standard calibrations. In the absence of a more thorough real-time calibration, we estimate that the precision of the 5-min averaged CO measurements is 5–10 ppb. Ozone (O_3) mixing ratio was monitored using a Thermo Environmental Instruments (TEI) 49C analyzer and measurements were recorded as 1-min averages. The O_3 measurements were not calibrated during the campaign, and the concentrations relative to the campaign average were reported.

3 Results

This section describes the meteorological conditions under which carboxylic acid groups are formed, the composition of organic mass quantified through complementary measurements by FTIR, AMS, and STXM-NEXAFS. The daily variations in carboxylic acid and alkane groups are discussed. To help to understand these variations, components contributing to organic mass are identified from factor analysis.

3.1 Meteorological conditions during the sampling period

The sampling period was characterized by stable temperature and RH with the averages and standard deviations being $20.2 \pm 2.5^\circ\text{C}$ and $79.3 \pm 8.6\%$, respectively. Temperature peaked in the afternoon and showed a minimum in the early morning, anti-correlating with RH. Photosynthetically active radiation peaked at noon. Land-sea breeze circulation was observed during the measurement period and was consistent with previous studies (Hughes et al., 2007). In general, surface wind shifted at about 07:00 a.m. (from offshore to onshore wind) and 10:00 p.m. (from onshore to offshore wind).

Back trajectories were calculated hourly using the Hybrid Single-Particle Lagrangian Integrated Trajectory (HYSPLIT) model (Draxler and Rolph, 2003; Rolph, 2003) at 200 m and were used to determine the origin of air masses. The FTIR filter samples were grouped into sectors representing the origin of air masses as indicated by the top bars in Fig. 3a. Each air mass sector (along with consistent daytime onshore flow) allows analysis of particles originating from the same source region (most frequently the ports of Los Angeles and Long Beach) for a consistent number (1–3) of days. Example back trajectories associated with each sector are shown in Fig. 1. To further investigate likely sources of OM, potential source contribution function (PSCF) was applied to the factors resulted from factor analysis. PSCF classifies the back trajectories as “high” and “low” by concentration of the target component and calculates the probability that a source is located at a particular region (Pekney et al., 2006). Examples of PSCF results are shown in Fig. 5.

[Title Page](#)[Abstract](#)[Introduction](#)[Conclusions](#)[References](#)[Tables](#)[Figures](#)[◀](#)[▶](#)[◀](#)[▶](#)[Back](#)[Close](#)[Full Screen / Esc](#)[Printer-friendly Version](#)[Interactive Discussion](#)

3.2 Organic and inorganic compositions of submicron particles

Table 1 summarizes the campaign average concentrations of the FTIR and AMS-measured components. Figure 3a shows the time series and the average fraction of organic functional groups measured by FTIR. The OM concentration varied from 0.39 to 11 $\mu\text{g m}^{-3}$ with an average concentration of $3.3 \pm 1.9 \mu\text{g m}^{-3}$, which was comparable to the OM concentration in the summer of 2008 (Hawkins and Russell, 2010a) and about twice the OM concentration measured in the winter of 2009 (Day et al., 2010) at the same site. Alkane functional group concentration was $1.5 \pm 1.1 \mu\text{g m}^{-3}$ and contributed 47% of the OM. Carboxylic acid functional groups accounted for 34% of the OM with an average concentration of $1.1 \pm 0.8 \mu\text{g m}^{-3}$. The concentration of hydroxyl functional groups was $0.40 \pm 0.24 \mu\text{g m}^{-3}$, accounting for 12% of the OM. Amine, non-acid carbonyl, and organonitrate functional groups contributed small fractions to the OM (3%, 2%, and 2%, respectively). Alkene and aromatic functional groups were below detection limit for all samples and each was estimated to account for no more than 4% of the OM. These two functional groups were excluded from the analyses in this study. Samples associated with different air mass sectors had similar organic functional group compositions but differed in mass, with the Los Angeles-Long Beach port and the Riverside sectors containing significantly higher OM, indicating transport of pollutants from these heavily polluted regions to the sampling site, which is consistent with the findings of Ault et al. (2009). Only days associated with single air mass sector (32 out of 47 days) were included (Fig. 3a) in the diurnal cycle analysis in order to track the daily changes in compositions caused by chemistry rather than air mixing.

The non-refractory submicron particle mass (nrPM_{10}) concentration measured by the AMS showed similar variation to the FTIR OM concentration (Fig. 3b), indicating common sources or formation pathways of organic and inorganic compounds. Non-refractory OM (nrOM) was the largest component of nrPM_{10} (43%). Sulfate concentration was $3.1 \pm 1.7 \mu\text{g m}^{-3}$ and accounted for 39% of nrPM_{10} . Ammonium and nitrate contributed 12% and 5% of nrPM_{10} , respectively. Only non-refractory species of chloride

Ozone-driven formation of acid

S. Liu et al.

Title Page

Abstract

Introduction

Conclusions

References

Tables

Figures

◀

▶

◀

▶

Back

Close

Full Screen / Esc

Printer-friendly Version

Interactive Discussion



were measured by the AMS, and these accounted for a negligible amount of nrPM₁ with a mass fraction of 0.3% (Table 1).

The FTIR and AMS-measured OM compared reasonably well as shown in Fig. 4. The slope (1.1) and correlation coefficient ($r = 0.7$) of the OM correlation in this study fall into the typical ranges of the FTIR and AMS-measured OM comparison as summarized by Russell et al. (2009b) from eight previous field campaigns. These values are comparable to the average slope (1.1) and r (0.67) derived from the Scripps Summer 2008 and the Scripps Winter 2009 projects (Russell et al., 2009b). Pearson's correlation coefficient for a reduced major axis regression is used in this study. For samples associated with low sulfate fractions, the trend becomes more scattered from the 1:1 line and the sulfate-based CE has better agreement when sulfate accounts for more than 20% of nrPM₁. This is consistent with the fact that the sulfate-based CE used here was developed for ambient samples associated with relatively high sulfate fractions that were about 40% on average (Quinn et al., 2006).

3.3 Diurnal cycles of organic and inorganic components

For the diurnal cycle analyses, the concentrations were normalized by the enhancement of carbon monoxide (ΔCO) mixing ratio (with respect to the background or unpolluted CO mixing ratio measured at the site during the study). This background CO mixing ratio was determined as the y-intercept of the linear regression of CO versus OM (DeCarlo et al., 2008), which differed slightly for the FTIR OM and the AMS nrOM at 89 ppb and 80 ppb, respectively. The difference of the two intercepts results from the larger AMS nrOM (10% higher than the FTIR OM). Since the difference of the two intercepts is insignificant (10%), an average value of 85 ppb was used as the background CO mixing ratio. Normalizing the concentration by CO, which does not react significantly on timescales of a few days, is used to separate the variations caused by the change of combustion source strength and effective dilution rates with variable meteorological conditions (which vary with ΔCO) from changes associated with aerosol processing in the atmosphere (which do not vary with ΔCO) (De Gouw et al., 2005, 2008; Gilardoni et al., 2009; DeCarlo et al., 2010).

Ozone-driven formation of acid

S. Liu et al.

Title Page

Abstract

Introduction

Conclusions

References

Tables

Figures

◀

▶

◀

▶

Back

Close

Full Screen / Esc

Printer-friendly Version

Interactive Discussion



**Ozone-driven
formation of acid**

S. Liu et al.

Title Page

Abstract

Introduction

Conclusions

References

Tables

Figures

◀

▶

◀

▶

Back

Close

Full Screen / Esc

Printer-friendly Version

Interactive Discussion



The diurnal profiles of normalized carboxylic acid group concentrations are classified into four types based on their diurnal pattern (Fig. 6). The features for the four types are (1) the concentration continuously increased during the day and peaked at night (Type 1), (2) the peak concentration occurred in the afternoon (Type 2), (3) the concentration peaked both at noon and at night (Type 3), and (4) the peak concentration occurred at noon (Type 4). The corresponding alkane group diurnal profiles (for the same samples as in Types 1–4 shown in Fig. 6) resemble that of carboxylic acid groups (Fig. 6), indicating alkane and carboxylic acid groups likely were forming in the same molecules, at the same time, and condensing simultaneously.

The four types of diurnal profiles share similar properties that all showed higher concentrations during the solar maximum relative to the early morning period. However, Type 1 and Type 2 both increase from early morning till noon and then peak higher in the late afternoon (“Afternoon High”), but they differ in nighttime concentrations with Type 1 showing high and Type 2 showing low nighttime concentrations. Analogously, Type 3 and Type 4 have similar daytime patterns peaking at noon (“Noon High”) but differing nighttime concentrations. The variation in concentration at night could be explained by land-sea breeze circulations, with Type 3 having high and Type 4 having low nighttime concentrations. The diurnal variations of local wind directions for the four types of days are shown in Fig. 2. The difference in nighttime winds explains the differences between the low and high nighttime concentrations. Nighttime winds coming from the northwest dominated in Type 1 days while easterlies prevailed at night in Type 2 days. This change in wind direction likely resulted in Type 1 being more influenced by marine air masses and Type 2 being more influenced by land air masses at night. Similarly, the profile difference between Type 3 and Type 4 is likely caused by the differing influence of nighttime easterlies. In order to focus on the diurnal changes in chemical composition, our analysis has focused only on the daytime patterns allowing us to group the four types of diurnal cycles into two meta-classes: Type 1 and 2 are merged into the Class A (“Afternoon High”) with carboxylic acid group concentration peaked in the afternoon and similarly, Type 3 and 4 are merged into the Class

B (“Noon High”) with noon-high concentrations. The daytime variations of carboxylic groups are consistent with the profiles of O₃ mixing ratios (Fig. 6) for the individual types, with O₃ peaked in the afternoon for the “Afternoon High” cases (Types 1 and 2) and peaked at noon for the “Noon High” cases (Types 3 and 4), indicating O₃-driven acid formation mechanism.

Figure 7 shows diurnal profiles of the AMS-measured fragment *m/z* 44 and the AMS Aged Combustion factor (identified from the factor analysis in Sect. 3.4.2) divided into the “Afternoon High” (Type 1 and 2) and the “Noon High” (Type 3 and 4) days. Fragment *m/z* 44, which is CO₂⁺ and representative of highly oxygenated organic components, tracked well with the AMS Aged Combustion factor. These two components peaked in the afternoon (14:00–18:00) in the “Afternoon High” days and the peak concentrations extended from noon to the afternoon (10:00–18:00) in the “Noon High” days, which are reflected in the average diurnal profiles for the two classes and consistent with the diurnal profiles of carboxylic acid group concentrations. The daytime peaks of *m/z* 44 and the Aged Combustion factor indicate enhanced SOA formation during the day (De Gouw and Jimenez, 2009). Carboxylic acid group concentration correlated well with *m/z* 44 and the AMS Aged Combustion factor concentrations for both “Afternoon High” and “Noon High” classes (Fig. 8), with the latter having better correlation coefficients of both carboxylic acid groups to *m/z* 44 and to the Aged Combustion factor ($r = 0.8$) but similar slopes. The correlation of acid and *m/z* 44 indicates that for these organic compositions, carboxylic acid groups and *m/z* 44 were likely associated with the same molecules and same formation mechanisms.

To evaluate evidence for photochemical processing in single particles, the average X-ray absorption spectra of single particles are shown in Fig. 9. Twenty-one morning particles and sixteen afternoon particles (collected on the same days as the morning particles) were analyzed. The afternoon-particle spectrum was characterized by a flat and broad black carbon peak at 285 eV, a broad peak ranging from 287 to 289 eV (peaks at 288.7 eV) indicative of alkane (the shoulder at 287.7 eV) and carboxylic acid (288.7 eV) functional group absorption, a carbonate peak at 290.4 eV, and two potassium peaks

**Ozone-driven
formation of acid**

S. Liu et al.

Title Page

Abstract

Introduction

Conclusions

References

Tables

Figures

◀

▶

◀

▶

Back

Close

Full Screen / Esc

Printer-friendly Version

Interactive Discussion



**Ozone-driven
formation of acid**

S. Liu et al.

Title Page

Abstract

Introduction

Conclusions

References

Tables

Figures

◀

▶

◀

▶

Back

Close

Full Screen / Esc

Printer-friendly Version

Interactive Discussion



at 297.4 and 299.9 eV (Russell et al., 2002). These spectra are comparable to the spectrum of CaCO_3 (Hawkins and Russell, 2010b) except for the carboxylic acid group absorption, suggesting that carboxylic acid groups may condense on marine particles originating from marine calcareous phytoplankton (Hawkins and Russell, 2010b) when air masses passed over the ocean. Compared to the afternoon spectrum, the morning spectrum had a narrower and sharper black carbon peak with more variations at all energies. The graphite content of particles is represented by calculating the %sp² hybridization for each particle (Takahama et al., 2007). Morning particles were associated with greater %sp² hybridization than afternoon particles at a 84% confidence level, indicating morning particles were more influenced by primary emissions that likely included black carbon cores.

3.4 PMF factors

PMF (Paatero and Tapper, 1994) can be used to separate the contributions of different sources, each with characteristic compositions, to the multicomponent mixtures in ambient organic and inorganic particles (Pekney et al., 2006). We applied PMF to the FTIR spectra and the AMS-measured organic fragment concentrations separately to identify robust, linearly-independent components that compose the OM (Lanz et al., 2007; Russell et al., 2009a).

3.4.1 PMF of the FTIR spectra

The FTIR PMF input matrix consisted of 234 mass-weighted and baselined FTIR spectra. The scaling factors were estimated by baselining errors calculated using the automated algorithm described by Russell et al. (2009a). The robust mode was used and the outliers were downweighted during the fitting procedure. Two to six factors with an FPEAK-range of [0, ±0.2, ±0.4, ±0.6, ±0.8, ±1] were tested. The Q-value versus FPEAK plot showed a “U” shape with the lowest Q values corresponding to FPEAK of -0.2, 0, 0.2, 0.4, and 0.6, which resulted in the same factors. The edge-FPEAK

values (-0.6 , -0.4 , ± 0.8 , and ± 1) resulted in increased Q values, indicating increased residuals associated with the PMF model (Lanz et al., 2007). Because the sensitivity to rotation was negligible for $FPEAK = -0.2$, 0 , 0.2 , 0.4 , and 0.6 , $FPEAK = 0$ was selected to represent the solution.

Two- and three- factor solutions were excluded since only 85% of the OM was re-produced, while four or more factors reconstructed more than 95% of the OM. Cor-related factors ($r > 0.5$) with similar compositions were combined to one factor (Liu et al., 2009), resulting in three factors for each of the four-, five-, and six-factor solu-tions. The three recombined factors resulted from the six-factor solution were selected because these factors captured events that were associated with trajectories from either know wildfires and from Los Angeles-Long Beach ports. In addition, the factor profiles had similar peak structure ($r > 0.8$) with the known factors derived from the TEXAQS/GoMACCS 2006 and the Scripps Pier 2008 measurements (Hawkins and Russell, 2010a; Russell et al., 2009a).

The first factor spectrum correlated to the fossil fuel Combustion factor profiles of the TEXAQS/GoMACCS (Russell et al., 2009a) and the Scripps Pier 2008 measure-ments (Hawkins and Russell, 2010a) projects with r being 0.97 and 0.99, respectively, indicating similar organic compositions, likely resulting from similar sources or pro-cesses. This factor was characterized by large fractions and co-existence of alkane and carboxylic acid functional groups (51% and 42% of the factor OM, respectively) and was identified as a fossil fuel Combustion factor. The concentration of this factor was $3.0 \mu\text{g m}^{-3}$, accounting for 62% of the OM on average (Fig. 3c). Hydroxyl and amine functional groups contributed 7% and 1% of the factor OM, respectively. PSCF image (Fig. 5a) shows the origin of this factor was mainly located at the vicinity of Los Angeles region, which are dominated by fossil fuel combustion emissions. The second factor spectrum correlated to the Biomass Burning factor profiles identified from the TEXAQS/GoMACCS (Russell et al., 2009a) and the Scripps Pier 2008 measurements (Hawkins and Russell, 2010a) with $r = 0.87$ and 0.93 , respectively. The factor time series (Fig. 3c) showed three high concentration periods: 26 August–2 September,

**Ozone-driven
formation of acid**

S. Liu et al.

Title Page

Abstract

Introduction

Conclusions

References

Tables

Figures

◀

▶

◀

▶

Back

Close

Full Screen / Esc

Printer-friendly Version

Interactive Discussion



8–22 August, and 22–27 September, corresponding to the top three fires in acreage that occurred in California: the Station fire (in Los Angeles County), the La Brea fire (in Santa Barbara County), and the Guiberson fire (in Ventura County), respectively (http://www.fire.ca.gov/fire_protection/fire_protection_fire_info_redbooks_2009.php). PSCF image (Fig. 5b) indicates that this factor is likely from north of Los Angeles – Santa Barbara County, as well as Baja California regions, consistent with fire events that occurred during the sampling period and fire maps from satellite measurements (Fig. 5c). Based on the similarity of this factor spectrum to previously identified biomass burning factors and the increase during fire-influenced time periods, this factor was identified as a Biomass Burning factor. The factor concentration was $0.88 \mu\text{g m}^{-3}$ on average and accounted for 18% of the OM. Non-acid carbonyl and alkane functional groups dominated this factor, accounting for 44% and 34% of the factor OM, respectively. The factor spectrum of the third factor was comparable ($r = 0.82$) to the spectrum of the polluted marine factor described in the Scripps Pier 2008 measurements (Hawkins and Russell, 2010a) and was nearly identical to a sample of seawater atomized and collected for FTIR analysis (Gaston, 2011). This factor was identified as a Marine factor that accounted for 20% of the OM on average and was dominated by hydroxyl functional groups (72%). Alkane, carboxylic acid, and amine functional groups contributed 20%, 4%, and 3% of the OM, respectively. The concentration and composition of the factors are summarized in Table 2.

3.4.2 PMF of organic fragment concentrations

The input matrix and the error files for PMF of the AMS measurements were prepared using the Igor Pro 5 (Wavemetrics Inc.) codes based on the work of Zhang et al. (2005). Two to six factors with FPEAK-range of $[0, \pm 0.2, \pm 0.4, \pm 0.6, \pm 0.8, \pm 1]$ were investigated. The Q-value versus FPEAK plot shows a “U” shape with the lowest Q values corresponding to FPEAK of $-0.2, 0, \text{ and } 0.2$. The factors generated for each rotation were nearly indistinguishable. FPEAK = 0 was selected to represent the solutions. A distinct factor with significant mass was missing when two factors were

Ozone-driven formation of acid

S. Liu et al.

[Title Page](#)[Abstract](#)[Introduction](#)[Conclusions](#)[References](#)[Tables](#)[Figures](#)[◀](#)[▶](#)[◀](#)[▶](#)[Back](#)[Close](#)[Full Screen / Esc](#)[Printer-friendly Version](#)[Interactive Discussion](#)

used. For each of the four-, five-, and six-factor solutions, highly correlated factors ($r > 0.7$) were combined, resulting in three recombined factors, which resembled the three factors generated from the three-factor solution, indicating factors were split into smaller but indistinguishable components when more than three factors were used.

5 The three-factor solution was selected and 98% of the OM was reproduced.

The factors were identified by comparing normalized factor spectra with the online AMS reference spectra (Ulbrich et al., 2007, 2009). The first factor spectrum correlated to several LV-OOA (low-volatility OOA) and SOA profiles. For example, the factor spectrum correlated to the Pittsburgh OOA factor profile (Zhang et al., 2005; $r = 0.93$ for $m/z > 44$ and $r = 0.95$ for all m/z) and SOA profile from the photooxidation of *m*-xylene with seed aerosols under RH = 55% (Bahreini et al., 2005; $r = 0.94$ for $m/z > 44$ and $r = 0.90$ for all m/z). The factor could not be further split into LV-OOA and SV-OOA (semi-volatile OOA) factors as shown in many previous studies (Ng et al., 2010), likely because of the relatively low particle concentration at the sampling site. The diurnal cycle of this factor showed a significant increase in concentration during the day and decrease in the morning and night (Fig. 7b), indicating photochemical origins of this factor. This factor likely represented an aged component formed from processed primary emissions. The factor was identified as an Aged Combustion factor, which accounted for 61% of the AMS nrOM and was associated with the largest m/z 44 nrOM fraction and m/z 44 to m/z 43 ratio among all factors (Table 2). The second factor profile strongly correlated with the wood burning spectrum ($r = 0.90$ for both $m/z > 44$ for all m/z) identified by Lanz et al. (2007) and the brush fire spectrum ($r = 0.94$ for $m/z > 44$ and $r = 0.92$ for all m/z) described by Bahreini et al. (2005). This factor was identified as a Biomass Burning factor, accounting for 26% of the nrOM. No correlation was found between the third factor spectrum and the spectra from the AMS database. The factor concentration correlated to none of the concentrations of the AMS-measured inorganic compounds. The factor profile correlated moderately ($r = 0.5$) with the Arctic Organic Aerosol (AOA) factor (which likely originates from the ocean) from the ICEALOT study (Frossard et al., 2011) and the time series correlated to that of the FTIR Marine factor

**Ozone-driven
formation of acid**

S. Liu et al.

Title Page

Abstract

Introduction

Conclusions

References

Tables

Figures

◀

▶

◀

▶

Back

Close

Full Screen / Esc

Printer-friendly Version

Interactive Discussion



with $r = 0.5$. This factor likely represented a Marine factor, which accounted for 13% of the nrOM.

3.4.3 Comparison of PMF factors identified from the FTIR and AMS measurements

5 The reconstructed OM from the FTIR and the AMS PMF analyses correlated with $r = 0.7$ and a slope of 1.1 (with the FTIR OM 10% higher). A Combustion factor, a Biomass Burning factor, and a Marine-derived factor were identified from both the FTIR and the AMS PMF analyses. The Combustion factors dominated the OM (approximately 60%) from both analyses and the time series correlated to each other with

10 $r = 0.5$ and a slope of 1.2 (FTIR factor OM was 20% higher). The Biomass Burning factors resulted from the FTIR and the AMS measurements correlated with $r = 0.7$ and slope = 0.9 (FTIR factor OM was 10% lower). The OM fractions of the two Biomass Burning factors agreed with less than 10% difference, well within the expected accuracies of both FTIR and AMS OM. The two Marine factors correlated to each other with

15 $r = 0.5$, with the FTIR factor OM higher by a factor of 2.1. The weaker correlation and the lower mass of the AMS Marine factor may be caused by a low collection efficiency for organic compounds on NaCl particles as well as a lack of marine-aerosol specific fragments in the AMS measurements. Alternatively it could result from lower absorptivity of carbohydrate hydroxyl groups relative to the hydroxyl standards employed in

20 the quantification algorithm (Russell et al., 2009a). In summary, the factors identified by PMF analyses of the FTIR and the AMS measurements agreed well and the mass differences were within 30% except for the Marine factor. The good agreement shows the consistency of the measurements and the robustness of the identified factors.

Ozone-driven formation of acid

S. Liu et al.

Title Page

Abstract

Introduction

Conclusions

References

Tables

Figures

◀

▶

◀

▶

Back

Close

Full Screen / Esc

Printer-friendly Version

Interactive Discussion



4 Discussion

In this section, we discuss carboxylic acid functional group formation mechanisms based on evidence from the diurnal profiles and size distributions. We use this evidence to estimate the SOA mass fraction in submicron particles associated with the different PMF factors. In addition, we identify factors that drive the variability in hydroxyl functional groups.

4.1 Photochemical formation of carboxylic acids

The daytime concentration of carboxylic acid groups tightly followed the variations of O_3 mixing ratios (Fig. 6). The two components correlated well with a correlation coefficient of 0.7 (Fig. 10). The correlation of carboxylic acid groups and odd oxygen ($O_3 + NO_2$) could be better (Herndon et al., 2008), however, the NO_2 measurements were not available in this study. Atmospheric O_3 mixing ratio is affected by a number of parameters, including meteorological variables such as solar intensity, temperature, and RH and gas-phase chemical compositions such as NO_x , volatile organic compounds (VOC), and other factors (Kleinman et al., 1994; Liu et al., 1994; Talbot et al., 2005). Days with afternoon O_3 peaks (the “Afternoon High” days) and noon O_3 peaks (the “Noon High” days) were associated with comparable variations and magnitudes of meteorological conditions, including temperature, ambient RH, wind direction and speed, and photosynthetically active radiation, suggesting the peak time of O_3 mixing ratio was likely affected by other parameters, such as NO_x and VOC mixing ratios (for which the measurements were not available).

The diurnal covariation of carboxylic acids and O_3 provides substantial evidence for an O_3 -driven oxidation that forms carboxylic acid groups. The potential precursors of carboxylic acids in anthropogenic source dominated regions include alkanes and aromatics, which are emitted from fossil fuel combustion activities. Smog chamber studies show that OH oxidation of aromatics yields multifunctional group products with low alkane group mole fractions (<0.3) and higher non-acid carbonyl group mole fractions

[Title Page](#)[Abstract](#)[Introduction](#)[Conclusions](#)[References](#)[Tables](#)[Figures](#)[◀](#)[▶](#)[◀](#)[▶](#)[Back](#)[Close](#)[Full Screen / Esc](#)[Printer-friendly Version](#)[Interactive Discussion](#)

**Ozone-driven
formation of acid**

S. Liu et al.

Title Page

Abstract

Introduction

Conclusions

References

Tables

Figures

◀

▶

◀

▶

Back

Close

Full Screen / Esc

Printer-friendly Version

Interactive Discussion



(Kleindienst et al., 1999; Russell et al., 2011). Large mole fraction of alkane groups (0.85) and the absence of non-acid carbonyl groups of the FTIR Combustion factor rule out the aromatics as acid formation precursors. The carboxylic acid, hydroxyl, non-acid carbonyl, and alkane groups mole fractions of the Combustion factor were 0.11, 0.04, 0.00, and 0.85, comparable to the C₁₂ alkane oxidation products with mole fractions of 0.12, 0.13, 0.02, and 0.73 estimated by Russell et al. (2011), suggesting that alkanes are likely carboxylic acid formation precursors. Russell et al. (2011) hypothesize a two-step oxidation of gas-phase alkanes to form carboxylic acids. First, gas-phase alkanes are oxidized by OH radicals to form particle-phase dihydrofuran via H-atom subtraction, isomerization, cyclization, and dehydration processes. Second, dihydrofurans evaporate into the gas phase and react with O₃, producing products that are expected to be similar to cyclic alkene oxidation products, namely multi-functional products with carboxylic acid functional groups (which would be expected to partition into the particle phase due to their low vapor pressures). This mechanism explains the co-variation of particle-phase carboxylic acid groups and alkane groups, and the similarity of their diurnal trends to O₃ mixing ratios in this measurement, suggesting carboxylic acids are second-generation products of alkane oxidation.

Representative size distributions of *m/z* 44 and the AMS nrOM are shown in Fig. 11 for the “Afternoon High” days (for time period of 14:00–18:00) and the “Noon High” days (for time period of 10:00–14:00). For both cases, the size distributions of the two components showed similar variations and both peaked around 300–500 nm. The OM fraction of *m/z* 44 was nearly independent of particle size, while nrOM/nrPM₁ decreased with increasing particle diameter, comparable with a theoretical model of a surface-driven process (as shown in Fig. 11 iii and iv). The deviations from the model likely result from density differences of newly condensed mass. This type of size distribution is consistent with the “Condensation and Volume-limited Oxidation” mechanism proposed by Maria et al. (2004), indicating the condensation of newly formed nrOM onto existing particles (the mass fraction of nrOM increased with 1/D_p) and more *m/z* 44 were formed by further volume-limited oxidation in the particle phase (the mass of

m/z 44 scaled with particle volume), which likely occurred under high RH conditions constantly observed at the coastal sampling site. However, a correlation of m/z 44 concentrations to ambient RH was not observed, likely because of a lack of RH dynamic range since the RH was consistently high ($79.3 \pm 8.6\%$) during the observation period.

Several chamber studies have suggested acid-catalyzed formation of SOA (Edney et al., 2005; Kleindienst et al., 2006; Surratt et al., 2007), while others have observed the opposite (Bahreini et al., 2005; Tan et al., 2009). Zhang et al. (2007) investigated acidity effects on Pittsburgh SOA and concluded that no enhancement of SOA was observed during high acidity measurement periods. For this study, when the molar equivalence ratio of ammonium to sulfate plus nitrate was used as a surrogate for the acidity of aerosol particles (Quinn et al., 2006), there was no correlation of acidity with carboxylic acid functional group concentration, although particles are in acidic conditions.

4.2 SOA mass fraction

The contributions to SOA from carboxylic acid groups and OOA are both estimated by assuming that the minimum concentration which occurs in the early morning is representative of a background value (either from other sources or from processing on previous days) and that the increase that occurs (relative to ΔCO) is from photochemical processing in the atmosphere during a 12-h daytime in a single day. The background and diurnal cycles of carboxylic acid groups and the Combustion factors from the FTIR and AMS measurements are shown in Fig. 12. The SOA mass fraction calculation is summarized in Table 3.

In general, the SOA fractions are comparable for the “Afternoon High” and the “Noon High” days with the differences within 30%. The 12-h daytime increase in carboxylic acid group mass in the “non-morning” periods compared to the low during the morning period approximately accounted for 30% of the carboxylic acid group mass and 10% of OM; similarly the photochemical increase in the FTIR Combustion factor accounted for 28% of the factor mass and 17% of the OM. The AMS Aged Combustion factor showed

Ozone-driven formation of acid

S. Liu et al.

Title Page

Abstract

Introduction

Conclusions

References

Tables

Figures

◀

▶

◀

▶

Back

Close

Full Screen / Esc

Printer-friendly Version

Interactive Discussion



**Ozone-driven
formation of acid**

S. Liu et al.

[Title Page](#)[Abstract](#)[Introduction](#)[Conclusions](#)[References](#)[Tables](#)[Figures](#)[◀](#)[▶](#)[◀](#)[▶](#)[Back](#)[Close](#)[Full Screen / Esc](#)[Printer-friendly Version](#)[Interactive Discussion](#)

higher SOA mass fractions (41% and 23% for the factor mass and the OM, respectively) than the FTIR Combustion factor, but the two are within the measurement uncertainties of both of the techniques. The lower SOA fractions from acid-group-only-based estimates could be explained by the fact that the molecules contain other components besides the carboxylic acid groups (i.e. likely alkane groups; Lim and Ziemann, 2009). Comparing the estimates from the functional groups and the Combustion factors, we find that approximately 45–70% of the SOA molecules may be attributed to carboxylic acid groups and the remaining would be constituted by other organic functional groups.

4.3 Sources and characteristics of hydroxyl functional groups

Hydroxyl functional groups were mainly from marine sources, since their variation was uncorrelated with sulfate and the AMS and FTIR Combustion factors. Larger contributions from the hydroxyl groups and hence the Marine factor were associated with onshore winds from 07:00 to 22:00 (Fig. 13), which could bring concentrated marine aerosols to the sampling site, indicating the hydroxyl functional group concentration was modulated by the land-sea breeze circulation at the coastal site. The Marine factor concentration weakly correlated with local wind speed ($r = 0.3$ during onshore winds), consistent with the expected increase in particle production from wind-related bubble bursting on the ocean surface (Russell et al., 2010) but sufficiently influenced by other variables to mask a one-to-one link.

5 Conclusions

Measurements at the Scripps Pier showed that OM accounted for nearly 50% of ambient submicron particle mass. The OM was dominated by fossil fuel combustion type sources, which resulted in a mixture of alkane and carboxylic acid functional groups. In this mixture, the abundances of these two functional groups changed diurnally, with the carboxylic acid group concentration increasing significantly during the daytime,

**Ozone-driven
formation of acid**

S. Liu et al.

Title Page

Abstract

Introduction

Conclusions

References

Tables

Figures

◀

▶

◀

▶

Back

Close

Full Screen / Esc

Printer-friendly Version

Interactive Discussion



5 indicating photochemical formation of carboxylic acid groups, consistent with past studies that have argued carboxylic acids are secondary. This daytime increase was tightly correlated with O_3 mixing ratios, suggesting O_3 played an important role in acid formation. A two-step alkane oxidation mechanism is consistent with the observed diurnal
10 variation of carboxylic acid groups and the composition of the Combustion factor resulted from the PMF analysis. In this mechanism, gas-phase alkane molecules are oxidized by OH radicals, forming dihydrofuran in the particle phase, followed by evaporation of dihydrofuran and further gas-phase oxidation by O_3 . The O_3 peaked both at noon and in the afternoon, likely caused by different NO_x or VOC conditions upstream, resulting in two classes of carboxylic acid group and alkane group daytime profiles (the “Afternoon High” and the “Noon High” days) under comparable meteorological conditions. In both cases, the size distribution of m/z 44/nrOM and nrOM/PM₁ revealed that the newly formed nrOM condensed onto existing particles, while m/z 44 may undergo further reactions in the particle phase under high RH at the sampling site.

15 The fraction of OM that is contributed by secondary carboxylic acid groups is estimated to be 10%. This number represents a lower-bound of the SOA contribution to OM, as other groups are also present in photochemically-generated molecules (i.e. alkane groups). Another estimate is to consider the fraction of OOA that is formed each day as secondary, which is 15–30% of OM. These measurements account for only the
20 SOA formed during an approximately 12-h period, yet it contributes a large fraction of the combustion-associated OM factors (50% for FTIR) and a significant fraction of OM at the Scripps Pier during this study. This large contribution of alkane-derived SOA is not surprising given their large contributions to VOC emissions in the LA/LB source region and the relative absence of significant additional organic precursors during transit
25 in the coastal marine boundary layer. Our study reinforces the importance of gas-phase alkane photochemistry for the air quality of regions downwind of emission sources.

Acknowledgements. CO measurements were funded by the California Air Resources Board. We appreciate the fundings from UCSD-PNNL ACCI and NSF grant ATM-0744636. We also thank Kimberly Prather and Cassandra Gaston for providing the O_3 data.

References

- Altieri, K., Carlton, A., Lim, H., Turpin, B., and Seitzinger, S.: Evidence for oligomer formation in clouds: Reactions of isoprene oxidation products, *Environ. Sci. Technol.*, 40, 4956–4960, 2006. 7191
- 5 Ault, A., Moore, M., Furutani, H., and Prather, K.: Impact of emissions from the Los Angeles port region on san diego air quality during regional transport events, *Environ. Sci. Technol.*, 43, 3500–3506, 2009. 7196
- Bahreini, R., Keywood, M., Ng, N., Varutbangkul, V., Gao, S., Flagan, R., Seinfeld, J., Worsnop, D., and Jimenez, J.: Measurements of secondary organic aerosol from oxidation of cycloalkenes, terpenes, and m-xylene using an Aerodyne aerosol mass spectrometer, *Environ. Sci. Technol.*, 39, 5674–5688, 2005. 7203, 7207
- 10 Blando, J. and Turpin, B.: Secondary organic aerosol formation in cloud and fog droplets: a literature evaluation of plausibility, *Atmos. Environ.*, 34, 1623–1632, 2000. 7191
- Claeys, M., Szmigielski, R., Kourtchev, I., Van der Veken, P., Vermeylen, R., Maenhaut, W., Jaoui, M., Kleindienst, T., Lewandowski, M., Offenberg, J., and Edney, E. O.: Hydroxydicarboxylic acids: Markers for secondary organic aerosol from the photooxidation of α -pinene, *Environ. Sci. Technol.*, 41, 1628–1634, 2007. 7191
- 15 Day, D., Liu, S., Russell, L., and Ziemann, P.: Organonitrate group concentrations in submicron particles with high nitrate and organic fractions in coastal southern California, *Atmos. Environ.*, 44, 1970–1979, 2010. 7193, 7196
- De Gouw, J. and Jimenez, J.: Organic aerosols in the Earth's atmosphere, *Environ. Sci. Technol.*, 43, 7614–7618, 2009. 7199
- De Gouw, J., Middlebrook, A., Warneke, C., Goldan, P., Kuster, W., Roberts, J., Fehsenfeld, F., Worsnop, D., Canagaratna, M., Pszenny, A., Keene, W. C., Marchewka, M., Bertman, S. B., and Bates, T. S.: Budget of organic carbon in a polluted atmosphere: Results from the New England Air Quality Study in 2002, *J. Geophys. Res.-Atmos.*, 110, D16305, doi:10.1029/2004JD005623, 2005. 7197
- 25 De Gouw, J., Brock, C., Atlas, E., Bates, T., Fehsenfeld, F., Goldan, P., Holloway, J., Kuster, W., Lerner, B., Matthew, B., Middlebrook, A. M., Onasch, T. B., Peltier, R. E., Quinn, P. K., Senff, C. J., Stohl, A., Sullivan, A. P., Trainer, M., Warneke, C., Weber, R. J., and Williams, E. J.: Sources of particulate matter in the northeastern United States in summer: 1. Direct emissions and secondary formation of organic matter in urban plumes, *J. Geophys. Res.*-
- 30

Ozone-driven formation of acid

S. Liu et al.

Title Page

Abstract

Introduction

Conclusions

References

Tables

Figures

◀

▶

◀

▶

Back

Close

Full Screen / Esc

Printer-friendly Version

Interactive Discussion



**Ozone-driven
formation of acid**

S. Liu et al.

Title Page

Abstract

Introduction

Conclusions

References

Tables

Figures

◀

▶

◀

▶

Back

Close

Full Screen / Esc

Printer-friendly Version

Interactive Discussion



Atmos., 113, D08301, doi:10.1029/2007JD009243, 2008. 7197

DeCarlo, P. F., Dunlea, E. J., Kimmel, J. R., Aiken, A. C., Sueper, D., Crouse, J., Wennberg, P. O., Emmons, L., Shinozuka, Y., Clarke, A., Zhou, J., Tomlinson, J., Collins, D. R., Knapp, D., Weinheimer, A. J., Montzka, D. D., Campos, T., and Jimenez, J. L.: Fast airborne aerosol size and chemistry measurements above Mexico City and Central Mexico during the MILAGRO campaign, *Atmos. Chem. Phys.*, 8, 4027–4048, doi:10.5194/acp-8-4027-2008, 2008. 7197

DeCarlo, P. F., Ulbrich, I. M., Crouse, J., de Foy, B., Dunlea, E. J., Aiken, A. C., Knapp, D., Weinheimer, A. J., Campos, T., Wennberg, P. O., and Jimenez, J. L.: Investigation of the sources and processing of organic aerosol over the Central Mexican Plateau from aircraft measurements during MILAGRO, *Atmos. Chem. Phys.*, 10, 5257–5280, doi:10.5194/acp-10-5257-2010, 2010. 7197

Draxler, R. and Rolph, G.: HYSPLIT (HYbrid Single-Particle Lagrangian Integrated Trajectory) Model access via NOAA ARL READY Website (<http://www.arl.noaa.gov/ready/hysplit4.html>), NOAA Air Resources Laboratory, Silver Spring, 2003. 7195

Edney, E., Kleindienst, T., Jaoui, M., Lewandowski, M., Offenber, J., Wang, W., and Claeys, M.: Formation of 2-methyl tetrols and 2-methylglyceric acid in secondary organic aerosol from laboratory irradiated isoprene/NO_x/SO₂/air mixtures and their detection in ambient PM_{2.5} samples collected in the eastern United States, *Atmos. Environ.*, 39, 5281–5289, 2005. 7207

Ervens, B., Feingold, G., Frost, G., and Kreidenweis, S.: A modeling study of aqueous production of dicarboxylic acids: 1. Chemical pathways and speciated organic mass production, *J. Geophys. Res.-Atmos.*, 109, D15205, doi:10.1029/2003JD004387, 2004. 7191

Fisseha, R., Dommen, J., Sax, M., Paulsen, D., Kalberer, M., Maurer, R., H"ofler, F., Weingartner, E., and Baltensperger, U.: Identification of organic acids in secondary organic aerosol and the corresponding gas phase from chamber experiments, *Anal. Chem.*, 76, 6535–6540, 2004. 7191

Fraser, M., Yue, Z., Tropp, R., Kohl, S., and Chow, J.: Molecular composition of organic fine particulate matter in Houston, TX, *Atmos. Environ.*, 36, 5751–5758, 2002. 7191

Frossard, A. A., Shaw, P. M., Russell, L. M., Kroll, J. H., Canagarna, M., Worsnop, D., Quinn, P. K., and Bates, T. S.: Springtime Arctic Haze Contributions of Submicron Organic Particles from European and Asian Combustion Sources, *J. Geophys. Res.-Atmos.*, in press, 2011. 7203

Fuzzi, S., Andreae, M. O., Huebert, B. J., Kulmala, M., Bond, T. C., Boy, M., Doherty, S. J.,

**Ozone-driven
formation of acid**

S. Liu et al.

Title Page

Abstract

Introduction

Conclusions

References

Tables

Figures

◀

▶

◀

▶

Back

Close

Full Screen / Esc

Printer-friendly Version

Interactive Discussion



Guenther, A., Kanakidou, M., Kawamura, K., Kerminen, V.-M., Lohmann, U., Russell, L. M., and Pöschl, U.: Critical assessment of the current state of scientific knowledge, terminology, and research needs concerning the role of organic aerosols in the atmosphere, climate, and global change, *Atmos. Chem. Phys.*, 6, 2017–2038, doi:10.5194/acp-6-2017-2006, 2006. 7190

Gaston, C. J.: Chemical Characterization of Marine Aerosol Generated by Bubble Bursting Natural and Artificial Seawater Solutions, in preparation, 2011. 7202

Gilardoni, S., Liu, S., Takahama, S., Russell, L. M., Allan, J. D., Steinbrecher, R., Jimenez, J. L., De Carlo, P. F., Dunlea, E. J., and Baumgardner, D.: Characterization of organic ambient aerosol during MIRAGE 2006 on three platforms, *Atmos. Chem. Phys.*, 9, 5417–5432, doi:10.5194/acp-9-5417-2009, 2009. 7197

Gray, H., Cass, G., Huntzicker, J., Heyerdahl, E., and Rau, J.: Characteristics of atmospheric organic and elemental carbon particle concentrations in Los Angeles, *Environ. Sci. Technol.*, 20, 580–589, 1986. 7192

Grosjean, D., Van Cauwenberghe, K., Schmid, J., Kelley, P., and Pitts Jr., J.: Identification of C3-C10 aliphatic dicarboxylic acids in airborne particulate matter, *Environ. Sci. Technol.*, 12, 313–317, 1978. 7191

Hallquist, M., Wenger, J. C., Baltensperger, U., Rudich, Y., Simpson, D., Claeys, M., Dommen, J., Donahue, N. M., George, C., Goldstein, A. H., Hamilton, J. F., Herrmann, H., Hoffmann, T., Iinuma, Y., Jang, M., Jenkin, M. E., Jimenez, J. L., Kiendler-Scharr, A., Maenhaut, W., McFiggans, G., Mentel, Th. F., Monod, A., Prvt, A. S. H., Seinfeld, J. H., Surratt, J. D., Szmigielski, R., and Wildt, J.: The formation, properties and impact of secondary organic aerosol: current and emerging issues, *Atmos. Chem. Phys.*, 9, 5155–5236, doi:10.5194/acp-9-5155-2009, 2009. 7191

Hawkins, L. N. and Russell, L. M.: Oxidation Of Ketone Groups In Transported Biomass Burning Aerosol From The 2008 Northern California Lightning Series Fires, *Atmos. Environ.*, 44, 4142–4154, 2010a. 7196, 7201, 7202

Hawkins, L. N. and Russell, L. M.: Polysaccharides, Proteins, and Phytoplankton Fragments: Four Chemically Distinct Types of Marine Primary Organic Aerosol Classified by Single Particle Spectromicroscopy, *Adv. Meteorol.*, 2010, 612132, doi:10.1155/2010/612132, 2010b. 7200

Herndon, S., Onasch, T., Wood, E., Kroll, J., Canagaratna, M., Jayne, J., Zavala, M., Knighton, W., Mazzoleni, C., Dubey, M., Ulbrich, I. M., Jimenez, J. L., Seila, R., de Gouw J. A.,

**Ozone-driven
formation of acid**

S. Liu et al.

Title Page

Abstract

Introduction

Conclusions

References

Tables

Figures

◀

▶

◀

▶

Back

Close

Full Screen / Esc

Printer-friendly Version

Interactive Discussion



de Foy, B., Fast, J., Molina, L. T., Kolb, C. E., and Worsnop, D. R.: Correlation of secondary organic aerosol with odd oxygen in Mexico City, *Geophys. Res. Lett.*, 35, L15804, doi:10.1029/2008GL034058, 2008. 7205

Hughes, M., Hall, A., and Fovell, R.: Dynamical controls on the diurnal cycle of temperature in complex topography, *Clim. Dynam.*, 29, 277–292, 2007. 7195

Jayne, J., Leard, D., Zhang, X., Davidovits, P., Smith, K., Kolb, C., and Worsnop, D.: Development of an aerosol mass spectrometer for size and composition analysis of submicron particles, *Aerosol. Sci. Tech.*, 33, 49–70, 2000. 7193

Kawamura, K.: Identification of C2-C10. omega.-oxocarboxylic acids, pyruvic acid, and C2-C3. alpha.-dicarbonyls in wet precipitation and aerosol samples by capillary GC and GC/MS, *Anal. Chem.*, 65, 3505–3511, 1993. 7191

Kawamura, K. and Gagosian, R.: Implications of ω -oxocarboxylic acids in the remote marine atmosphere for photo-oxidation of unsaturated fatty acids, *Nature*, 325, 330–332, 1987. 7191

Kawamura, K. and Ikushima, K.: Seasonal changes in the distribution of dicarboxylic acids in the urban atmosphere, *Environ. Sci. Technol.*, 27, 2227–2235, 1993. 7191

Kawamura, K. and Yasui, O.: Diurnal changes in the distribution of dicarboxylic acids, ketocarboxylic acids and dicarbonyls in the urban Tokyo atmosphere, *Atmos. Environ.*, 39, 1945–1960, 2005. 7191

Kleindienst, T., Smith, D., Li, W., Edney, E., Driscoll, D., Speer, R., and Weathers, W.: Secondary organic aerosol formation from the oxidation of aromatic hydrocarbons in the presence of dry submicron ammonium sulfate aerosol, *Atmos. Environ.*, 33, 3669–3681, 1999. 7206

Kleindienst, T., Edney, E., Lewandowski, M., Offenberg, J., and Jaoui, M.: Secondary organic carbon and aerosol yields from the irradiations of isoprene and α -pinene in the presence of NO_x and SO₂, *Environ. Sci. Technol.*, 40, 3807–3812, 2006. 7207

Kleinman, L., Lee, Y., Springston, S., Nunnermacker, L., Zhou, X., Brown, R., Hallock, K., Klotz, P., Leahy, D., Lee, J., and Newman, L.: Ozone formation at a rural site in the southeastern United States, *J. Geophys. Res.-Atmos.*, 99, 3469–3482, doi:10.1029/93JD02991, 1994. 7205

Lanz, V. A., Alfarra, M. R., Baltensperger, U., Buchmann, B., Hueglin, C., and Prvt, A. S. H.: Source apportionment of submicron organic aerosols at an urban site by factor analytical modelling of aerosol mass spectra, *Atmos. Chem. Phys.*, 7, 1503–1522, doi:10.5194/acp-7-1503-2007, 2007. 7200, 7203

**Ozone-driven
formation of acid**

S. Liu et al.

Title Page

Abstract

Introduction

Conclusions

References

Tables

Figures

◀

▶

◀

▶

Back

Close

Full Screen / Esc

Printer-friendly Version

Interactive Discussion



- Lim, Y. and Ziemann, P.: Chemistry of secondary organic aerosol formation from OH radical-initiated reactions of linear, branched, and cyclic alkanes in the presence of NO_x, *Aerosol. Sci. Tech.*, 43, 604–619, 2009. 7191, 7208
- 5 Liu, C., Huang, C., Shieh, S., and Wu, C.: Important meteorological parameters for ozone episodes experienced in the Taipei basin, *Atmos. Environ.*, 28, 159–173, 1994. 7205
- Liu, S., Takahama, S., Russell, L. M., Gilardoni, S., and Baumgardner, D.: Oxygenated organic functional groups and their sources in single and submicron organic particles in MILAGRO 2006 campaign, *Atmos. Chem. Phys.*, 9, 6849–6863, doi:10.5194/acp-9-6849-2009, 2009. 7191, 7194, 7201
- 10 Maria, S., Russell, L., Turpin, B., and Porcja, R.: FTIR measurements of functional groups and organic mass in aerosol samples over the Caribbean, *Atmos. Environ.*, 36, 5185–5196, 2002. 7191
- Maria, S., Russell, L., Gilles, M., and Myneni, S.: Organic aerosol growth mechanisms and their climate-forcing implications, *Science*, 306, 1921–1924, 2004. 7194, 7206, 7231
- 15 Miracolo, M., Presto, A., Lambe, A., Hennigan, C., Donahue, N., Kroll, J., Worsnop, D., and Robinson, A.: Secondary organic aerosol formation from low-volatility organic vapors in motor vehicle emissions, *Environ. Sci. Technol.*, 44, 1638–1643, 2010. 7191
- Ng, N. L., Canagaratna, M. R., Zhang, Q., Jimenez, J. L., Tian, J., Ulbrich, I. M., Kroll, J. H., Docherty, K. S., Chhabra, P. S., Bahreini, R., Murphy, S. M., Seinfeld, J. H., Hildebrandt, L., Donahue, N. M., DeCarlo, P. F., Lanz, V. A., Prévôt, A. S. H., Dinar, E., Rudich, Y., and Worsnop, D. R.: Organic aerosol components observed in Northern Hemispheric datasets from Aerosol Mass Spectrometry, *Atmos. Chem. Phys.*, 10, 4625–4641, doi:10.5194/acp-10-4625-2010, 2010. 7203
- 20 Paatero, P. and Tapper, U.: Positive matrix factorization: A non-negative factor model with optimal utilization of error estimates of data values, *Environmetrics*, 5, 111–126, 1994. 7200
- 25 Pekney, N., Davidson, C., Robinson, A., Zhou, L., Hopke, P., Eatough, D., and Rogge, W.: Major Source Categories for PM 2.5 in Pittsburgh using PMF and UNMIX, *Aerosol. Sci. Tech.*, 40, 910–924, 2006. 7195, 7200
- Presto, A., Miracolo, M., Donahue, N., and Robinson, A.: Secondary organic aerosol formation from high-NO_x photo-oxidation of low volatility precursors: n-alkanes, *Environ. Sci. Technol.*, 44, 2029–2034, 2010. 7191
- 30 Quinn, P., Bates, T., Coffman, D., Onasch, T., Worsnop, D., Baynard, T., De Gouw, J., Goldan, P., Kuster, W., Williams, E., Roberts, J. M., Lerner, B., Stohl, A., Pettersson, A., and Love-

**Ozone-driven
formation of acid**

S. Liu et al.

Title Page

Abstract

Introduction

Conclusions

References

Tables

Figures

◀

▶

◀

▶

Back

Close

Full Screen / Esc

Printer-friendly Version

Interactive Discussion



joy, R. E.: Impacts of sources and aging on submicrometer aerosol properties in the marine boundary layer across the Gulf of Maine, *J. Geophys. Res.-Atmos.*, 111, D23S36, doi:10.1029/2006JD007582, 2006. 7193, 7197, 7207

Rogge, W., Mazurek, M., Hildemann, L., Cass, G., and Simoneit, B.: Quantification of urban organic aerosols at a molecular level: identification, abundance and seasonal variation, *Atmos. Environ.*, 27, 1309–1330, 1993. 7191

Rolph, G.: Real-time Environmental Applications and Display sYstem (READY) Website (<http://www.arl.noaa.gov/ready/hysplit4.html>), NOAA Air Resources Laboratory, Silver Spring, Silver Spring, MD, 2003. 7195

Russell, L. M., Maria, S., and Myneni, S.: Mapping organic coatings on atmospheric particles, *Geophys. Res. Lett.*, 29, 1779, doi:10.1029/2002GL014874, 2002. 7194

Russell, L. M., Takahama, S., Liu, S., Hawkins, L., Covert, D., Quinn, P., and Bates, T.: Oxygenated fraction and mass of organic aerosol from direct emission and atmospheric processing measured on the R/VRonald Brown during TEXAQS/GoMACCS 2006, *J. Geophys. Res.-Atmos.*, 114, D00F05, doi:10.1029/2008JD011275, 2009a. 7191, 7193, 7200, 7201, 7204

Russell, L. M., Bahadur, R., Hawkins, L., Allan, J., Baumgardner, D., Quinn, P., and Bates, T.: Organic aerosol characterization by complementary measurements of chemical bonds and molecular fragments, *Atmos. Environ.*, 43, 6100–6105, 2009b. 7197

Russell, L. M., Hawkins, L. N., Frossard, A., Quinn, P., and Bates, T.: Carbohydrate-like composition of submicron atmospheric particles and their production from ocean bubble bursting, *P. Natl. Acad. Sci.*, 107, 6652, doi:10.1073/pnas.0908905107, 2010. 7208

Russell, L. M., Bahadur, R., and Ziemann, P. J.: Identifying organic aerosol sources by comparing functional group composition in chamber and atmospheric particles, *P. Natl. Acad. Sci.*, doi:10.1073/pnas.1006461108, 2011. 7191, 7206

Sullivan, A. and Weber, R.: Chemical characterization of the ambient organic aerosol soluble in water: 1. Isolation of hydrophobic and hydrophilic fractions with a XAD-8 resin, *J. Geophys. Res.-Atmos.*, 111, D05314, doi:10.1029/2005JD006485, 2006. 7191

Sullivan, R. and Prather, K.: Investigations of the diurnal cycle and mixing state of oxalic acid in individual particles in Asian aerosol outflow, *Environ. Sci. Technol.*, 41, 8062–8069, 2007. 7191

Surratt, J., Lewandowski, M., Offenberg, J., Jaoui, M., Kleindienst, T., Edney, E., and Seinfeld, J.: Effect of acidity on secondary organic aerosol formation from isoprene, *Environ. Sci.*

**Ozone-driven
formation of acid**

S. Liu et al.

Title Page

Abstract

Introduction

Conclusions

References

Tables

Figures

◀

▶

◀

▶

Back

Close

Full Screen / Esc

Printer-friendly Version

Interactive Discussion



Technol., 41, 5363–5369, 2007. 7207

Takahama, S., Gilardoni, S., Russell, L., and Kilcoyne, A.: Classification of multiple types of organic carbon composition in atmospheric particles by scanning transmission X-ray microscopy analysis, *Atmos. Environ.*, 41, 9435–9451, 2007. 7200

5 Takahama, S., Liu, S., and Russell, L.: Coatings and clusters of carboxylic acids in carbon-containing atmospheric particles from spectromicroscopy and their implications for cloud-nucleating and optical properties, *J. Geophys. Res.-Atmos.*, 115, D01202, doi:10.1029/2009JD012622, 2010. 7194

10 Talbot, R., Mao, H., and Sive, B.: Diurnal characteristics of surface level O₃ and other important trace gases in New England, *J. Geophys. Res.-Atmos.*, 110, D09307, doi:10.1029/2004JD005449, 2005. 7205

Tan, Y., Perri, M., Seitzinger, S., and Turpin, B.: Effects of Precursor Concentration and Acidic Sulfate in Aqueous Glyoxal- OH Radical Oxidation and Implications for Secondary Organic Aerosol, *Environ. Sci. Technol.*, 43, 8105–8112, 2009. 7207

15 Turpin, B., Huntzicker, J., Larson, S., and Cass, G.: Los Angeles summer midday particulate carbon: primary and secondary aerosol, *Environ. Sci. Technol.*, 25, 1788–1793, 1991. 7192

Turpin, B., Saxena, P., and Andrews, E.: Measuring and simulating particulate organics in the atmosphere: problems and prospects, *Atmos. Environ.*, 34, 2983–3013, 2000. 7190

20 Ulbrich, I. M., Canagaratna, M. R., Zhang, Q., Worsnop, D. R., and Jimenez, J. L.: Interpretation of organic components from Positive Matrix Factorization of aerosol mass spectrometric data, *Atmos. Chem. Phys.*, 9, 2891–2918, doi:10.5194/acp-9-2891-2009, 2009. 7203

Ulbrich, I. M., Lechner, M., and Jimenez, J. L.: AMS Spectral Database, <http://www.xyz.org/~jones/idx.g.htm>, access:10Feb2010, 2007. 7203

25 Wang, G., Niu, S., Liu, C., and Wang, L.: Identification of dicarboxylic acids and aldehydes of PM₁₀ and PM_{2.5} aerosols in Nanjing, China, *Atmos. Environ.*, 36, 1941–1950, 2002. 7191

Wang, G., Kawamura, K., Xie, M., Hu, S., Gao, S., Cao, J., An, Z., and Wang, Z.: Size-distributions of n-alkanes, PAHs and hopanes and their sources in the urban, mountain and marine atmospheres over East Asia, *Atmos. Chem. Phys.*, 9, 8869–8882, doi:10.5194/acp-9-8869-2009, 2009. 7191

30 Warneck, P.: In-cloud chemistry opens pathway to the formation of oxalic acid in the marine atmosphere, *Atmos. Environ.*, 37, 2423–2427, 2003. 7191

Yu, J., Griffin, R., Cocker, D., Flagan, R., Seinfeld, J., and Blanchard, P.: Observation of gaseous and particulate products of monoterpene oxidation in forest atmospheres, *Geo-*

**Ozone-driven
formation of acid**

S. Liu et al.

[Title Page](#)[Abstract](#)[Introduction](#)[Conclusions](#)[References](#)[Tables](#)[Figures](#)[I◀](#)[▶I](#)[◀](#)[▶](#)[Back](#)[Close](#)[Full Screen / Esc](#)[Printer-friendly Version](#)[Interactive Discussion](#)

phys. Res. Lett., 26, 1145–1148, doi:10.1029/1999GL900169, 1999. 7191, 7192

Yu, J., Huang, X., Xu, J., and Hu, M.: When aerosol sulfate goes up, so does oxalate: implication for the formation mechanisms of oxalate, Environ. Sci. Technol., 39, 128–133, 2005. 7191

5 Zhang, Q., Alfarra, M., Worsnop, D., Allan, J., Coe, H., Canagaratna, M., and Jimenez, J.: Deconvolution and quantification of hydrocarbon-like and oxygenated organic aerosols based on aerosol mass spectrometry, Environ. Sci. Technol., 39, 4938–4952, 2005. 7202

Zhang, Q., Jimenez, J., Worsnop, D., and Canagaratna, M.: A case study of urban particle acidity and its influence on secondary organic aerosol, Environ. Sci. Technol., 41, 3213–
10 3219, 2007. 7207

Zhang, Y. Y., Müller, L., Winterhalter, R., Moortgat, G. K., Hoffmann, T., and Pöschl, U.: Seasonal cycle and temperature dependence of pinene oxidation products, dicarboxylic acids and nitrophenols in fine and coarse air particulate matter, Atmos. Chem. Phys., 10, 7859–
7873, doi:10.5194/acp-10-7859-2010, 2010. 7191

Ozone-driven
formation of acid

S. Liu et al.

Table 1. Campaign average and standard deviation of FTIR-measured OM, FTIR organic functional group concentrations, and AMS-measured OM, sulfate, ammonium, nitrate, and chloride concentrations in μm^{-3} . Functional group OM mass fractions (for FTIR) and component PM₁ mass fractions (for AMS) are shown in the parentheses.

FTIR	OM	3.3 ± 1.9
	Alkane	1.5 ± 1.1 (47%)
	Carboxylic Acid	1.1 ± 0.77 (34%)
	Hydroxyl	0.40 ± 0.24 (12%)
	Amine	0.11 ± 0.09 (3%)
	Non-Acid Carbonyl	0.06 ± 0.21 (2%)
AMS	Organonitrate	0.07 ± 0.12 (2%)
	OM	3.9 ± 3.0 (43%)
	Sulfate	3.1 ± 1.7 (39%)
	Ammonium	1.0 ± 0.53 (12%)
	Nitrate	0.43 ± 0.49 (5%)
	Chloride	0.03 ± 0.05 (0.3%)

Title Page

Abstract

Introduction

Conclusions

References

Tables

Figures

I◀

▶I

◀

▶

Back

Close

Full Screen / Esc

Printer-friendly Version

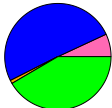
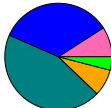
Interactive Discussion



Ozone-driven
formation of acid

S. Liu et al.

Table 2. Concentration and composition of PMF factors identified from the FTIR and the AMS measurements. Colors in the pie charts indicate alkane (blue), carboxylic acid (green), hydroxyl (hot pink), amine (orange), and non-acid carbonyl (teal) functional groups. Mass fractions of the factors are shown in the parentheses.

		Aged Combustion	Biomass Burning	Marine Origin
FTIR	Concentration (μm^{-3})	3.0 (62%)	0.88 (18%)	0.97 (20%)
	O/C	0.46	0.48	1.04
	Composition			
AMS	Concentration (μm^{-3})	2.5 (61%)	1.1 (26%)	0.51 (13%)
	(<i>m/z</i> 44)/OM	26%	5%	2.6%
	(<i>m/z</i> 60)/OM	0.1%	0.1%	0.6%
	(<i>m/z</i> 44)/(<i>m/z</i> 43)	7.5	0.6	1.5
	(<i>m/z</i> 44)/(<i>m/z</i> 57)	146	2.7	3.6

Title Page

Abstract

Introduction

Conclusions

References

Tables

Figures

◀

▶

◀

▶

Back

Close

Full Screen / Esc

Printer-friendly Version

Interactive Discussion



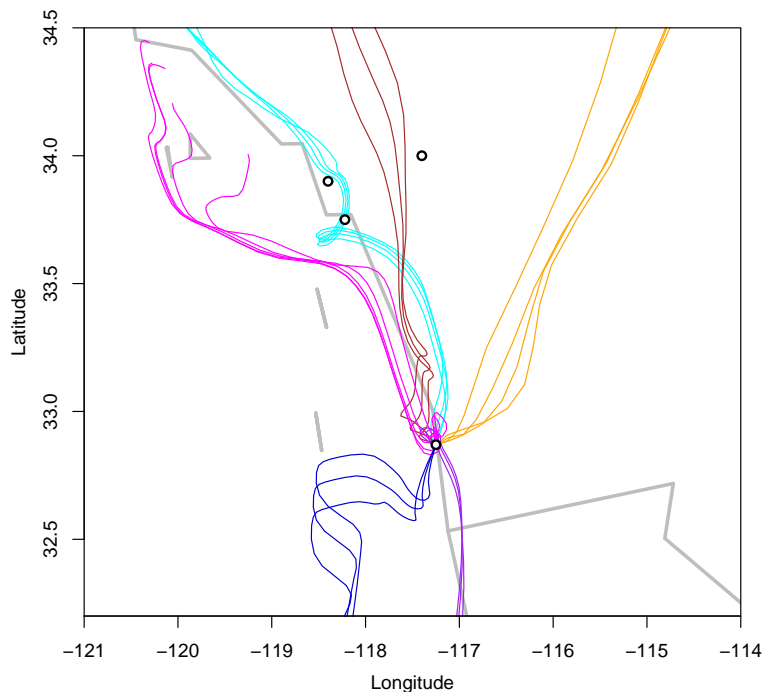


Fig. 1. Example back trajectories representing Los Angeles-Long Beach (cyan; air mass coming from Los Angeles and Long Beach regions), Riverside (brown; air mass originating from Riverside vicinity), Inland (orange; easterly/northeasterly air mass), Tijuana-Ensenada (purple; southerly air mass), Mixed coastal (magenta; northerly air mass coming along the coast of California), and Ocean (dark blue; westerly air mass) air mass sectors during the campaign. The black circles (from top to bottom) indicate Riverside, Los Angeles, Los Angeles - Long Beach port, and the sampling site.

Ozone-driven formation of acid

S. Liu et al.

Title Page	
Abstract	Introduction
Conclusions	References
Tables	Figures
◀	▶
◀	▶
Back	Close
Full Screen / Esc	
Printer-friendly Version	
Interactive Discussion	



**Ozone-driven
formation of acid**

S. Liu et al.

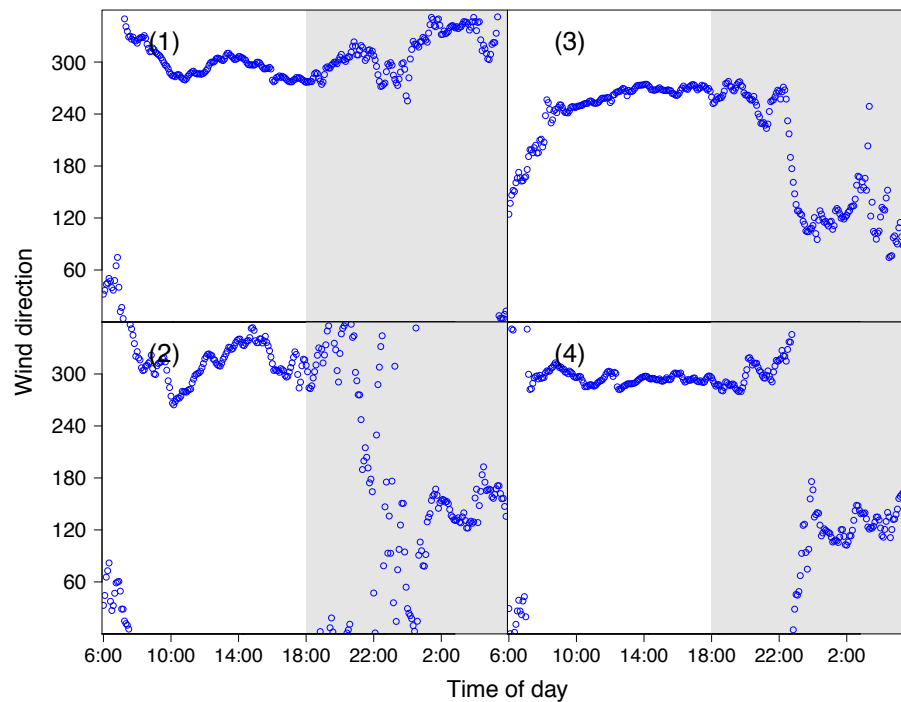


Fig. 2. Vector-averaged diurnal cycles of wind direction corresponding to the four types of days shown in Fig. 6. Shaded areas indicate nighttime periods.

[Title Page](#)[Abstract](#)[Introduction](#)[Conclusions](#)[References](#)[Tables](#)[Figures](#)[◀](#)[▶](#)[◀](#)[▶](#)[Back](#)[Close](#)[Full Screen / Esc](#)[Printer-friendly Version](#)[Interactive Discussion](#)

Ozone-driven
formation of acid

S. Liu et al.

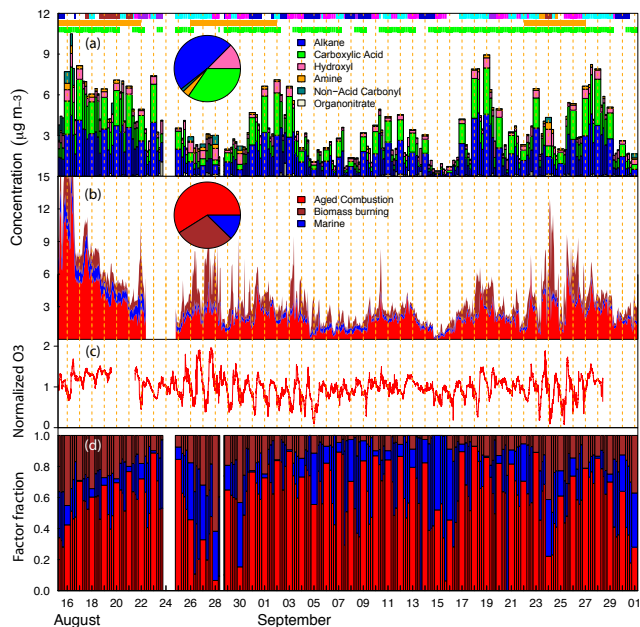


Fig. 3. (a) Time series of organic functional group concentrations measured by the FTIR; sectors are indicated by the top color bars (same colors as in Fig. 1), for which the sector associated with each FTIR sample was determined as the air mass origin shown by the majority (>80%) of the back trajectories during the sampling time; top brown bars indicate fire periods corresponding to the La Brea fire (in Santa Barbara County), the Station fire (in Los Angeles County), and the Guiberson fire (in Ventura County), respectively (from left to right); top green bars indicate samples associated with single air mass sector, which were used for diurnal profile analysis. (b) Time series of AMS factors identified by PMF analysis. The inner pie charts in (a) and (b) respectively show campaign average compositions of FTIR components and AMS factors. (c) Time series of normalized O_3 (normalized by campaign average) mixing ratio. (d) Mass fractions of the FTIR Combustion factor (red), the Biomass Burning factor (brown), and the Marine factor (blue) during the measurement.

Ozone-driven
formation of acid

S. Liu et al.

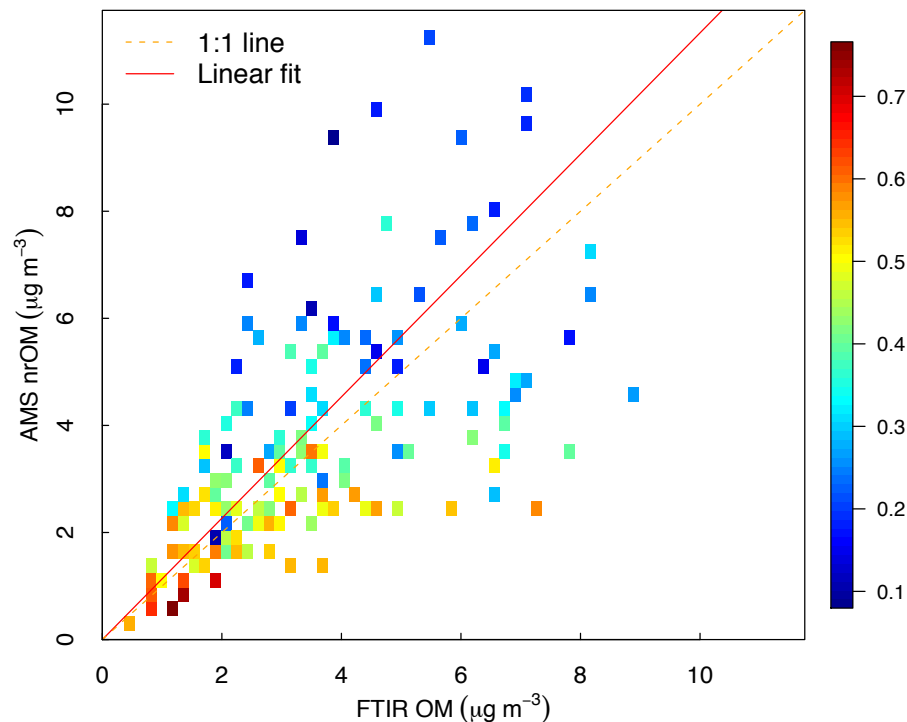


Fig. 4. Comparison of OM measured by the FTIR and the AMS. Colors indicate sulfate mass fraction of nrPM₁. Correlation coefficients for high sulfate mass samples (mass fraction >20%) and low sulfate mass samples (sulfate fraction <20%) are 0.8 and 0.6, respectively.

Title Page

Abstract

Introduction

Conclusions

References

Tables

Figures

◀

▶

◀

▶

Back

Close

Full Screen / Esc

Printer-friendly Version

Interactive Discussion



Ozone-driven
formation of acid

S. Liu et al.

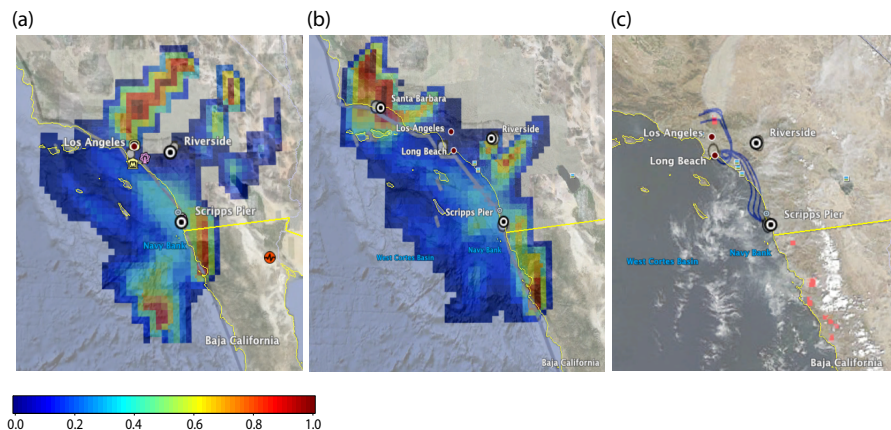


Fig. 5. Potential Source Contribution Function (PSCF) images of **(a)** the FTIR Combustion factor and **(b)** the FTIR Biomass Burning factor with warmer colors indicate higher probability. **(c)** Fire map on 29 August with red points showing fire spots and blue lines indicating back trajectories ending at the Scripps Pier. Fire image was obtained from NOAA's Aqua satellite.

Title Page

Abstract

Introduction

Conclusions

References

Tables

Figures

◀

▶

◀

▶

Back

Close

Full Screen / Esc

Printer-friendly Version

Interactive Discussion



Ozone-driven
formation of acid

S. Liu et al.

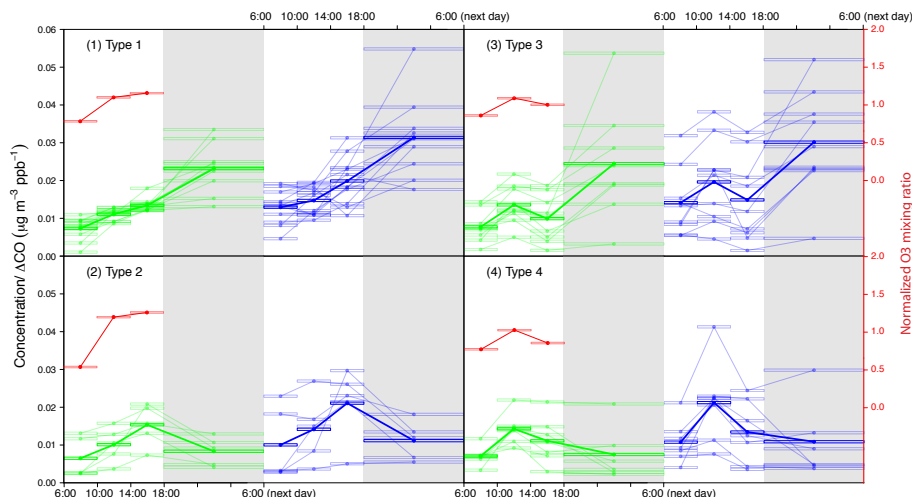


Fig. 6. Diurnal cycles of normalized carboxylic acid group concentrations (green) and alkane group concentrations (blue) divided into four types (1–4) shown in panels (1), (2), (3), and (4), respectively. Each rectangle represents one FTIR sample with the length of the rectangle indicating the sampling duration. The lines connecting the rectangles show samples collected in the same day. The thinner rectangles and lines represent daily diurnal profiles, while the thicker rectangles and lines show the averages for the days in the corresponding panel. The red dashed lines represent average diurnal profiles of normalized O_3 mixing ratio for the four types of days. Shaded areas indicate nighttime periods corresponding to the FTIR nighttime samples, which were excluded from the diurnal cycle analyses.

[Title Page](#)[Abstract](#)[Introduction](#)[Conclusions](#)[References](#)[Tables](#)[Figures](#)[◀](#)[▶](#)[◀](#)[▶](#)[Back](#)[Close](#)[Full Screen / Esc](#)[Printer-friendly Version](#)[Interactive Discussion](#)

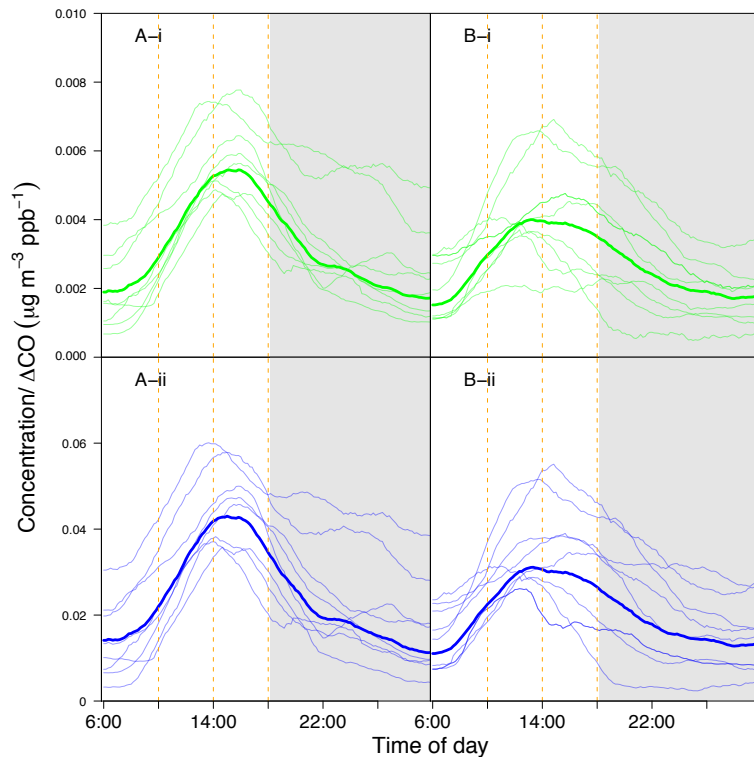


Fig. 7. Diurnal cycles of (i) m/z 44, and (ii) the AMS Aged Combustion factor for A (“Afternoon High”) and B (“Noon High”) cases. The thinner lines represent daily diurnal cycles and the thicker lines represent the averages. The curves are smoothed using the “Boxcar Smoothing” method with 30-point averaging to reduce high-frequency noise in the measurements. Shaded areas indicate nighttime periods.

Title Page

Abstract

Introduction

Conclusions

References

Tables

Figures

◀

▶

◀

▶

Back

Close

Full Screen / Esc

Printer-friendly Version

Interactive Discussion



Ozone-driven
formation of acid

S. Liu et al.

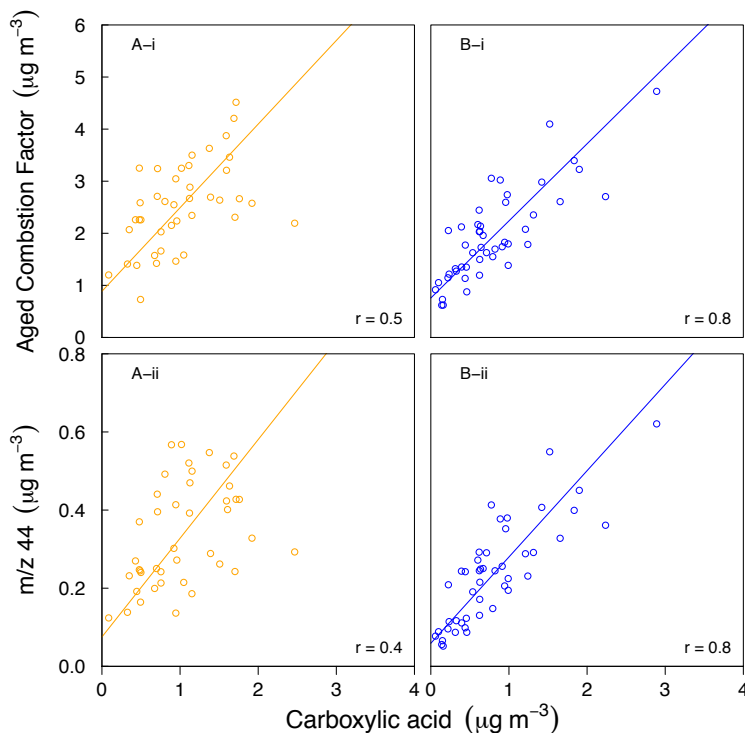


Fig. 8. Mass concentration correlation of carboxylic acid groups with (i) the AMS Aged Combustion factor and (ii) m/z 44 for A (“Afternoon High”) and B (“Noon High”) cases. The correlation coefficients are shown in the legends.

[Title Page](#)[Abstract](#)[Introduction](#)[Conclusions](#)[References](#)[Tables](#)[Figures](#)[◀](#)[▶](#)[◀](#)[▶](#)[Back](#)[Close](#)[Full Screen / Esc](#)[Printer-friendly Version](#)[Interactive Discussion](#)

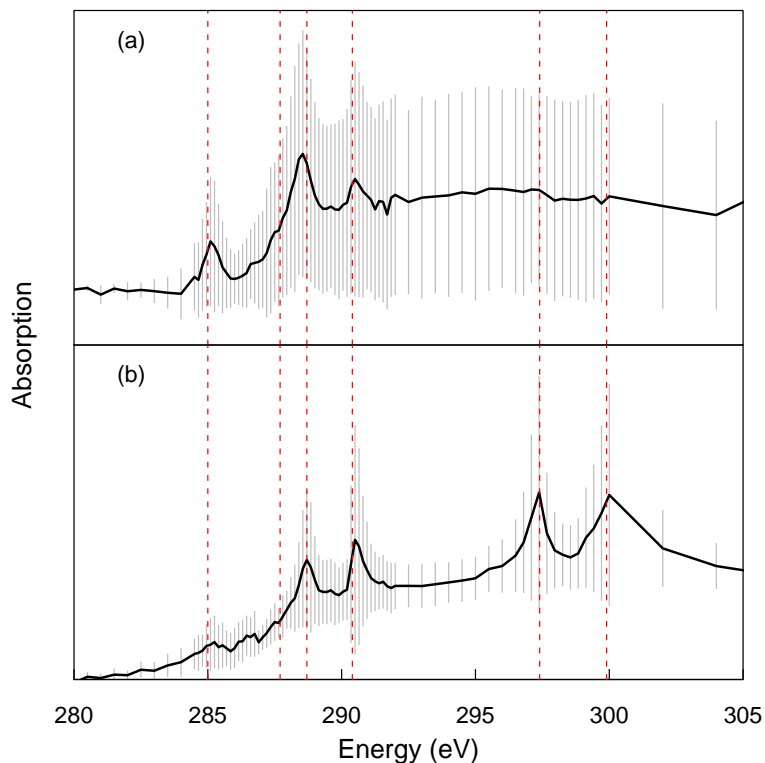


Fig. 9. Average X-ray spectra of **(a)** twenty-one morning and **(b)** sixteen afternoon particles. Grey vertical bars indicate the standard deviations of absorption at corresponding energies. Red vertical lines indicate alkene group (285 eV), alkane group (287.7 eV), carboxylic acid group (288.7 eV), carbonate (290.4 eV), and K (297.4 and 299.9 eV) absorptions.

Ozone-driven formation of acid

S. Liu et al.

Title Page

Abstract

Introduction

Conclusions

References

Tables

Figures

◀

▶

◀

▶

Back

Close

Full Screen / Esc

Printer-friendly Version

Interactive Discussion



**Ozone-driven
formation of acid**

S. Liu et al.

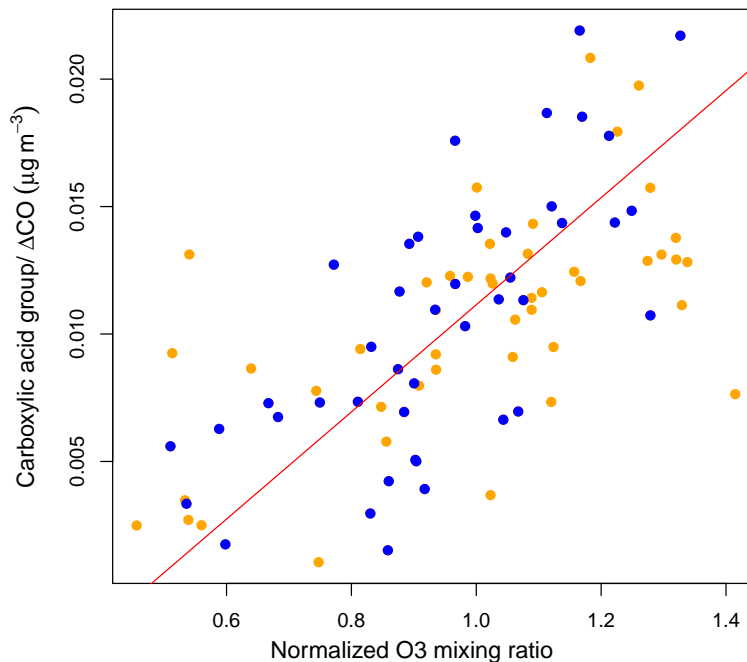


Fig. 10. Correlation of normalized carboxylic acid group concentration and normalized O₃ mixing ratio (by campaign average) for the “Afternoon High” (orange) and “Noon High” (blue) cases. The correlation coefficient is 0.7.

[Title Page](#)[Abstract](#)[Introduction](#)[Conclusions](#)[References](#)[Tables](#)[Figures](#)[◀](#)[▶](#)[◀](#)[▶](#)[Back](#)[Close](#)[Full Screen / Esc](#)[Printer-friendly Version](#)[Interactive Discussion](#)

Ozone-driven
formation of acid

S. Liu et al.

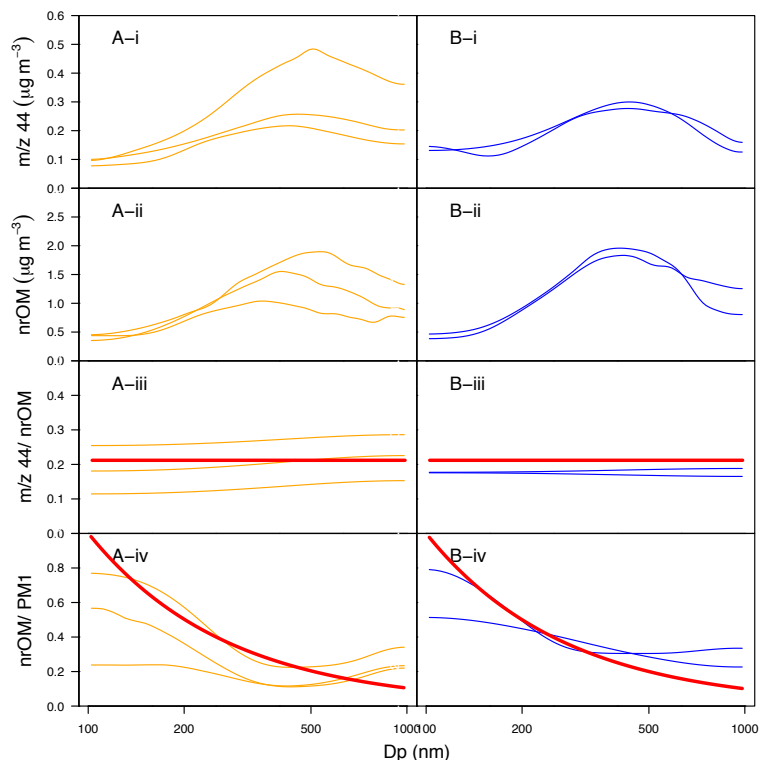


Fig. 11. Representative size distributions for A (“Afternoon High” days) on 12, 16, and 21 September, in time period 14:00–18:00 and B (“Noon High” days) on 17 and 20 September in time period 10:00–14:00 for (i) m/z 44, (ii) nrOM, (iii) m/z 44/nrOM, and (iv) nrOM/PM₁. The curves are smoothed with the “Boxcar Smoothing” method with 20-point averaging and wavelet de-noising method to reduce high-frequency noise in the measurements. Red lines are theoretical models representing (iii) constant with respect to particle diameter and (iv) inversely proportional to the particle diameter ($1/D_p$), for comparison to results of Maria et al. (2004).

Title Page

Abstract

Introduction

Conclusions

References

Tables

Figures

◀

▶

◀

▶

Back

Close

Full Screen / Esc

Printer-friendly Version

Interactive Discussion



Ozone-driven
formation of acid

S. Liu et al.

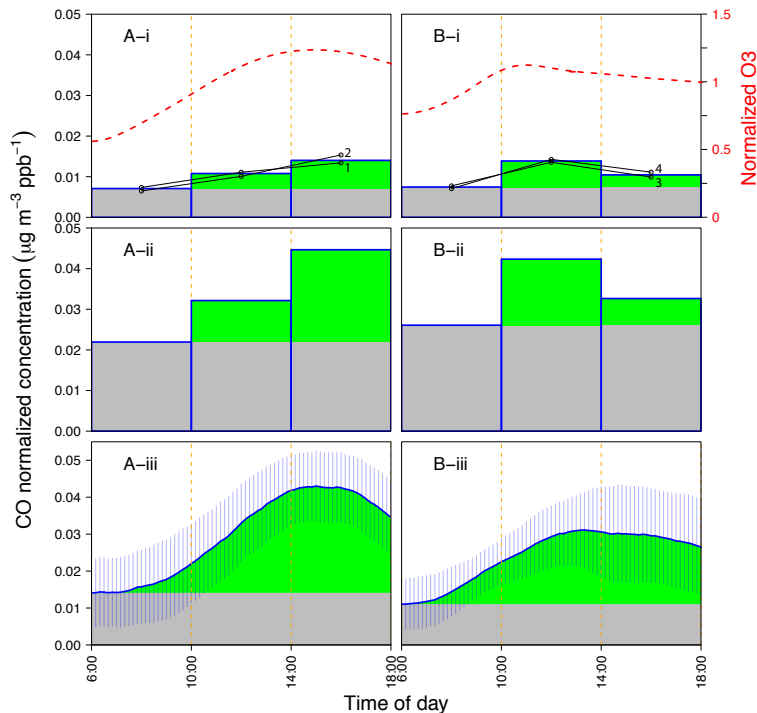


Fig. 12. Daytime profiles of A (“Afternoon High” days) and B (“Noon High” days) for (i) carboxylic acid group, (ii) the FTIR Combustion factor, and (iii) the AMS Aged Combustion factor concentration. Colors indicate POA (grey) and SOA (green), respectively. Red dashed lines in panels A-i and B-i represent average daytime profiles of normalized O_3 . Black lines in panels A-i and B-i are the average diurnal carboxylic acid group profiles corresponding to the four types shown in Fig. 6 as indicated by the numbers beside the lines. Vertical blue bars in panels A-ii and B-ii show standard deviations of the averaged diurnal cycles.

Title Page

Abstract

Introduction

Conclusions

References

Tables

Figures

◀

▶

◀

▶

Back

Close

Full Screen / Esc

Printer-friendly Version

Interactive Discussion



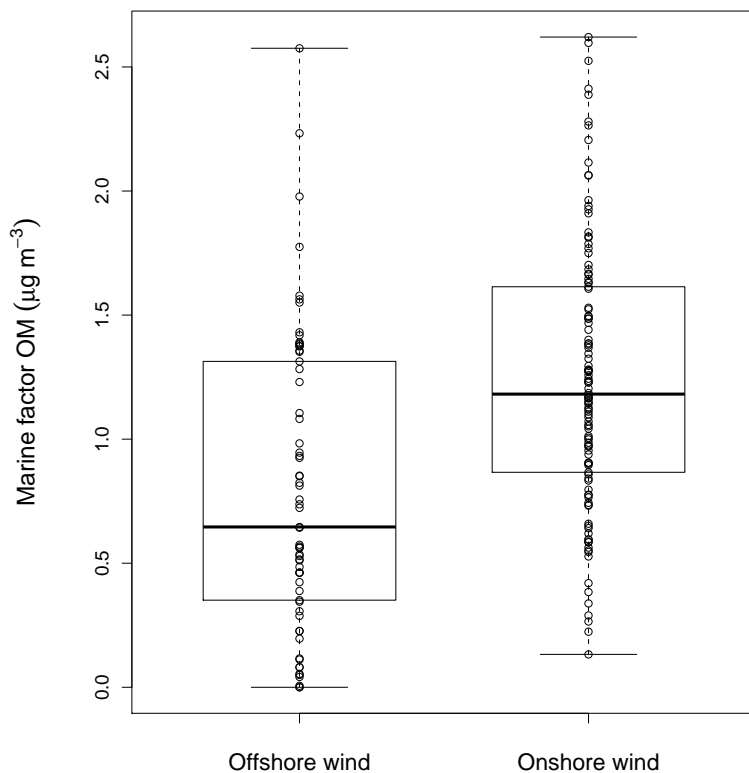


Fig. 13. The FTIR Marine factor concentration versus wind direction. 25th and 75th percentiles are shown by the upper and lower box bounds in each box. The points show individual samples. Median values are represented by the horizontal bars in the boxes.